A COUPLED CONTINUOUS/DISCONTINUOUS GALERKIN METHOD FOR THE SHALLOW WATER EQUATIONS

CLINT DAWSON*, DHARHAS POTHINA* AND JOANNES WESTERINK†

Abstract. We consider the approximation of the depth-averaged two dimensional shallow water equations by coupling a discontinuous Galerkin method for continuity with a continuous Galerkin method for momentum. The formulation is described in detail and numerical results on several test cases are presented. The discontinuous Galerkin method is locally conservative, flux-continuous on each element edge, and is suitable for both smooth and highly advective flows.

Key words. shallow water equations, Galerkin finite element method, discontinuous Galerkin method

1. Introduction. In this paper, we consider novel finite element methods for the numerical solution of the two-dimensional, depth-averaged shallow water equations (SWE).

Simulation of flow in shallow waters can be used, for example, to model environmental effects of dredging and commercial activities on fisheries and coastal wildlife, remediation of contaminated bays and estuaries for the purposes of improving water quality, modeling the effects of storm surges due to tropical storms and hurricanes, and studying freshwater-saltwater interactions.

The SWE model flow in domains whose characteristic wave length in the horizontal is much larger than the water depth [36]. The SWE consist of a first order hyperbolic continuity equation for the water elevation, coupled to momentum equations for the horizontal depth-averaged velocities. This system is referred to as the primitive form of the shallow water equations. These equations are often solved on domains with fairly irregular coastal boundaries. Furthermore, to avoid spurious boundary effects, it is often desirable to extend the domain away from the shore into deeper waters [39, 5].

Various finite element approaches have been developed for solving the SWE on such complex domains over the past two decades; see, for example, [32, 27, 26, 35, 42]. Much of this effort has been directed at deriving a finite element method which is stable and nonoscillatory under highly varying flow regimes, including advection dominant flows. As noted in [32], a straightforward use of equal order approximating spaces for elevation and velocity in the primitive SWE can lead to spurious spatial oscillations. Approaches based on mixed interpolation spaces [27] have met with limited success. A more widespread approach has been to replace the first order hyperbolic elevation equation with a second order hyperbolic "wave continuity equation," first proposed in [32]. This approach has served as the basis for numerous finite element studies, see for example, [28, 25, 24, 22, 23, 31, 37, 38, 39, 6, 5, 29, 40], and was analyzed in [8, 9].

The finite element methods mentioned above are based on continuous approximating spaces. The wave continuity formulation sacrifices the primitive continuity equation, thus the primitive form is no longer satisfied in a discrete sense. In recent

*Center for Subsurface Modeling - C0200; Texas Institute for Computational and Applied Mathematics; The University of Texas at Austin; Austin, TX 78712. This research was supported by NSF grant DMS-0107247.

†Dept. of Civil Engineering, University of Notre Dame, Notre Dame, IN.

years, finite element methods based on discretizing the primitive form of the SWE using discontinuous approximating spaces have been studied [2, 10, 1]. This discontinuous Galerkin (DG) approach has several appealing features; in particular, the ability to incorporate upwinding and stability post-processing (slope-limiting) into the solution to model highly advective flows, the ability to use different polynomial orders of approximation in different parts of the domain, and the ability to easily use nonconforming meshes (e.g., with hanging nodes). Moreover, the DG method is "locally conservative" and "flux-continuous," that is, the continuity equation relating the change in water elevation to water flux is satisfied in a weak sense element by element, and the numerical flux over each inter-element edge or face is continuous. These properties are useful when coupling the SWE to a transport equation for modeling, for example, contaminant migration [19]. DG methods have proven adept at modeling hyperbolic equations [16, 15, 14, 12, 18, 4], advection-diffusion [3, 17, 11, 20] and pure diffusion equations [41, 7, 33, 34]. See also [13] for a more thorough discussion on the history of DG methods. The disadvantage of DG methods over standard Galerkin methods is their cost: typically they require more degrees of freedom on a fixed mesh than their continuous counterparts.

In this paper, we present an approach for the SWE based on combining a DG method for continuity with a standard continuous Galerkin method for momentum. This approach allows us to model the hyperbolic continuity equation using the DG method, which is well-suited for this type of equation, while still using a continuous method for momentum. Therefore, we reduce the overall degrees of freedom versus using a complete DG method as in [1]. Stability and convergence results for this new methodology have recently been derived in [21]. Here we will focus on the numerical implementation of the method and its validation on some test problems.

We have implemented this approach into the Advanced Circulation Model (ADCIRC) [31], which uses the generalized wave continuity equation (GWCE) [28] for computing elevation. ADCIRC discretizes both the GWCE and the momentum equation using continuous, piecewise linear approximating functions defined on triangular elements. The GWCE finite element formulation does not produce a locally conservative, flux-continuous solution to the continuity equation. Moreover, the GWCE has no particular mechanism for handling highly advective flows. The GWCE does work quite well for smooth tidal flows, however, even those with so-called "$2\Delta x$" waves. In our implementation, we have essentially replaced the GWCE formulation with a DG method.

The paper is organized as follows. In the following section, we describe the mathematical model and the numerical approximation. Section three then contains numerical results on several two-dimensional test problems.

2. Problem definition. Vertical integration of the Navier–Stokes equations along with the assumptions of a hydrostatic pressure and a vertically uniform horizontal velocity profile results in the Shallow Water Equations (SWE) of the following form:

$$\frac{\partial \xi}{\partial t} + \nabla \cdot (\mathbf{u}H) = 0, \tag{1}$$

$$\frac{\partial \mathbf{u}}{\partial t} + \mathbf{u} \cdot \nabla \mathbf{u} + \tau_{bf}(\boldsymbol{u})\mathbf{u} + f_c \mathbf{k} \times \mathbf{u} + g\nabla \xi = \mathbf{F}. \tag{2}$$

(1) represents the conservation of mass and is also referred to as the primitive continuity equation; (2) represents the conservation of momentum in non-conservative

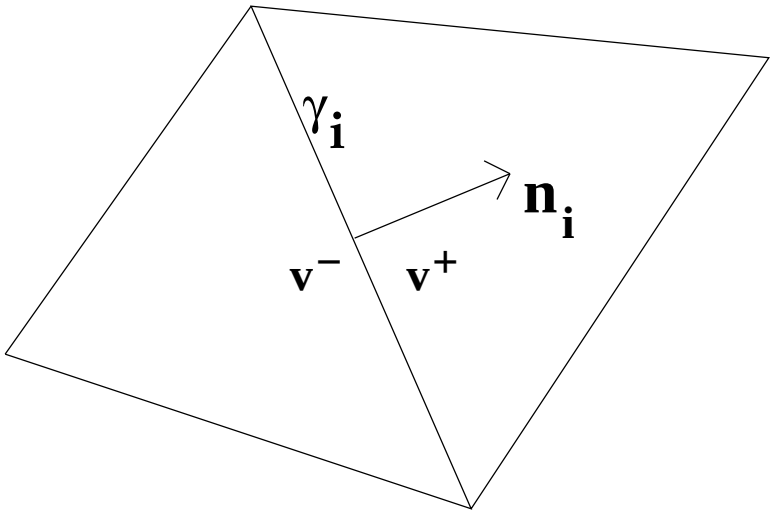

FIG. 1. *An edge γ_i with normal vector $\boldsymbol{n}_i$; v^- and v^+ are the values of v to the left and right of the edge, as determined by the normal $\boldsymbol{n}_i$.*

form. In the above equations, ξ represents the deflection of the air-liquid interface from the mean sea level, $H = h_b + \xi$ represents the total fluid depth, and h_b is the bathymetric depth, $\mathbf{u} = (u, v)$ is the depth averaged horizontal velocity field, f_c is the Coriolis parameter resulting from the earth's rotation, $\mathbf{k}$ is the local vertical vector, g is the gravitational acceleration, τ_{bf} is the bottom friction coefficient. Here we have neglected second order derivative terms in the momentum equation due to turbulent viscosity. In addition to the above described phenomena, often we need to include the effects of surface wind stress, variable atmospheric pressure and tidal potentials which are expressed through the body force $\mathbf{F}$ [36].

These equations are solved over a spatial domain Ω in $\mathbb{R}^2$ and for time $t > 0$. Let $\partial\Omega$ denote the boundary of Ω, where $\boldsymbol{n}$ is the fixed unit outward normal to $\partial\Omega$. Specified elevation and velocity and/or specified fluxes are assumed on $\partial\Omega$. Initial elevations and velocities ξ^0 and $\boldsymbol{u}^0$ at $t = 0$ must also be given.

Let $\{\mathcal{T}_h\}_{h>0}$ denote a triangulation of Ω such that no triangle Ω_e crosses $\partial\Omega$. We assume each element Ω_e has a element diameter h_e, with h being the maximal element diameter. Let $\mathcal{P}^k(\Omega_e)$ denote the space of complete polynomials of degree $k \geq 0$, defined on Ω_e.

For any function $v \in H^1(\Omega_e)$, for each element Ω_e, we denote its trace on interior edges γ_i by $v^{\pm}$, with

$$v^-(\mathbf{x}) = \lim_{s \to 0-} v(\mathbf{x} + s\boldsymbol{n}_i), \qquad v^+(\mathbf{x}) = \lim_{s \to 0+} v(\mathbf{x} + s\boldsymbol{n}_i),$$

where $\mathbf{x} \in \gamma_i$ and $\boldsymbol{n}_i$ denotes a fixed unit vector normal to γ_i, see Figure 1.

We will use the $L^2(R)$ inner product notation $(\cdot, \cdot)_R$ for domains $R \in \mathbb{R}^2$, and the notation $\langle u, v \rangle_R$ to denote integration over one-dimensional surfaces.

Multiply equation (1) by an arbitrary, test function $v \in H^1(\Omega_e)$ and integrate by parts over each element Ω_e to obtain

$$(\partial_t \xi, v)_{\Omega_e} - (\boldsymbol{u}\, H, \nabla v)_{\Omega_e} + \langle H\, \boldsymbol{u} \cdot \boldsymbol{n}_e, v \rangle_{\partial\Omega_e} = 0, \tag{3}$$

where $\boldsymbol{n}_e$ denotes the outward unit normal to the edge $\partial\Omega_e$.

Multiply equation (2) by a test function $\boldsymbol{w} \in (H^1(\Omega))^2$ and integrate over Ω to obtain,

$$(\frac{\partial \mathbf{u}}{\partial t} + \mathbf{u} \cdot \nabla \mathbf{u} + \tau_{bf}(\boldsymbol{u})\mathbf{u} + f_c \mathbf{k} \times \mathbf{u} + g\nabla\xi, \boldsymbol{w})_\Omega = (\mathbf{F}, \boldsymbol{w})_\Omega. \tag{4}$$

We approximate ξ in the polynomial space $V_h = \{v : v|_{\Omega_e} \in \mathcal{P}^k(\Omega_e)\}$, and we approximate each component of $\boldsymbol{u}$ in the subspace W_h of $H^1(\Omega)$, where W_h consists of continuous, piecewise linear polynomials. Denote these approximations by ξ_h and $\boldsymbol{u}_h$. We also will utilize a continuous approximation $\pi\xi_h \in W_h$ to ξ, defined below.

In continuous time, the scheme is outlined as follows:

- First, initial approximations $\xi_h(\cdot, 0) \in V_h$ and $\boldsymbol{u}_h(\cdot, 0) \in (W_h)^2$ are computed from the initial data ξ^0 and $\boldsymbol{u}^0$. This can be done by interpolation or L^2 projection.
- For $t > 0$, ξ_h is computed by

  $$(\partial_t \xi_h, v)_{\Omega_e} - (\boldsymbol{u}_h(\xi_h + h_b), \nabla v)_{\Omega_e} + \langle \mathbf{A}(\boldsymbol{u}_h; \xi_h^-, \xi_h^+) \cdot \boldsymbol{n}_e, v\rangle_{\partial\Omega_e} = 0, \quad v \in V_h. \tag{5}$$

  The numerical flux $\mathbf{A}(\boldsymbol{u}_h; \xi_h^-, \xi_h^+) \cdot \boldsymbol{n}_e \approx H\boldsymbol{u} \cdot \boldsymbol{n}_e$. We will discuss this term in detail below.
- ξ_h is then projected into the continuous space W_h by finding $\pi\xi_h \in W_h$ satisfying

  $$(\pi\xi_h, w)_\Omega = (\xi_h, w)_\Omega, \quad w \in W_h. \tag{6}$$

  In our implementation, mass lumping is used to approximate the integral on the left side of (6). Furthermore, on elevation specified boundary nodes, we set $\pi\xi_h$ to be equal to the specified elevation.
- Finally $\boldsymbol{u}_h$ is computed from (4) by

  $$\begin{aligned}(&\frac{\partial \boldsymbol{u}_h}{\partial t} + \boldsymbol{u}_h \cdot \nabla \mathbf{u}_h + \tau_{bf}(\boldsymbol{u}_h)\mathbf{u}_h \\ &+ f_c \mathbf{k} \times \mathbf{u}_h + g\nabla\pi\xi_h, \boldsymbol{w})_\Omega = (\mathbf{F}, \boldsymbol{w})_\Omega, \quad \boldsymbol{w} \in (W_h)^2.\end{aligned} \tag{7}$$

Note that (5) is conservative in the following sense: letting $v = 1$ on Ω_e and zero elsewhere, we find

$$\int_{\Omega_e} \partial_t \xi_h dx + \int_{\partial\Omega_e} \mathbf{A}(\boldsymbol{u}_h; \xi_h^-, \xi_h^+) \cdot \boldsymbol{n}_e ds = 0. \tag{8}$$

Thus, the change in elevation is balanced by the numerical flux $\mathbf{A} \cdot \boldsymbol{n}_e$ through the boundary of the element. As we will see below, this flux is uniquely defined (i.e., continuous) on each edge in the mesh. Thus, the DG scheme is both "locally conservative" and "flux continuous."

We now describe in more detail the implementation of the scheme above.

Implementation of (5). Though (5) is valid for any polynomial degree $k \geq 0$, we have implemented polynomials of order $k = 0$ and $k = 1$. For $k = 1$, we write

$$\xi_h|_{\Omega_e} \equiv \xi_{h,e} + \delta_x \xi_{h,e}(x - x_e) + \delta_y \xi_{h,e}(y - y_e), \tag{9}$$

where (x_e, y_e) is the barycenter of Ω_e. Thus, there are three degrees of freedom for ξ_h per element, and the basis functions for $\mathcal{P}^1(\Omega_e)$ are

$$\{1, x - x_e, y - y_e\}.$$

For $k = 0$, the x and y slope terms are omitted.

The time discretization of (5) is explicit. Given a time step $\Delta t > 0$ and initial approximations $(\xi_h(\cdot, t^n), \boldsymbol{u}_h(\cdot, t^n)) \equiv (\xi_h^n, \boldsymbol{u}_h^n)$, we integrate (5) forward in time using the explicit Euler method if $k = 0$, and using a second order Runge-Kutta method if $k = 1$. The second order Runge-Kutta method consists of computing two successive explicit Euler approximations, $\xi_h^{n,1}$ and $\xi_h^{n,2}$, keeping $\boldsymbol{u}_h^n$ fixed, and setting

$$\xi_h^{n+1} = \frac{1}{2}(\xi_h^n + \xi_h^{n,2}). \tag{10}$$

At each Euler step, a rudimentary slope limiter is applied to the slope terms $\delta_x \xi_{h,e}$ and $\delta_y \xi_{h,e}$ to minimize any overshoot or undershoot. In particular, we compute the values ξ_h^- and ξ_h^+ at the midpoint of each interior edge γ_i. If, for example, ξ_h^- does not lie between the constant values $\xi_{h,e}^-$ and $\xi_{h,e}^+$ on either side, the slope terms in Ω_e^- are set to zero, similarly for ξ_h^+.

The numerical flux $A(\boldsymbol{u}_h; \xi_h^-, \xi_h^+)$ is evaluated using the Roe flux outlined in [10, 30]. This flux is an upwind flux which has been used in many fluid applications with shocks and sharp gradients. In [10], we showed how to apply this flux when using a finite volume method (a DG method with $k = 0$) for both continuity and momentum. Here we only need to apply it to the continuity equation. Thus, we are only interested in the first component of this flux, which on edge γ_i, is defined as follows:

$$\begin{aligned}
\boldsymbol{n}_i &= (n_i^x, n_i^y) = \text{ normal vector to } \gamma_i, \\
H^{\pm} &= \xi_h^{\pm} + h_b, \\
\mathbf{q}^{\pm} &= \boldsymbol{u}_h H^{\pm}, \\
[\![H]\!] &= H^+ - H^-, \\
[\![\mathbf{q}]\!] &= ([\![q^x]\!], [\![q^y]\!]) = \mathbf{q}^+ - \mathbf{q}^-, \\
\hat{a} &= \sqrt{g(H^- + H^+)/2}, \\
\hat{\kappa} &= \sqrt{H^+/H^-}, \\
\hat{\boldsymbol{u}} &= \frac{\mathbf{q}^-}{(H^-)(1+\hat{\kappa})} + \frac{\mathbf{q}^+}{(H^+)(1+1/\hat{\kappa})}, \\
u_n &= \hat{\boldsymbol{u}} \cdot \boldsymbol{n}_i, \\
\lambda_1 &= \min(u_n - \hat{a}, 0), \\
\lambda_2 &= \min(u_n + \hat{a}, 0), \\
\alpha_1 &= \frac{(\hat{a} + u_n)[\![H]\!] - [\![\mathbf{q}]\!] \cdot \boldsymbol{n}_i}{2\hat{a}}, \\
\alpha_2 &= \frac{(\hat{a} - u_n)[\![H]\!] + [\![q^x]\!] \boldsymbol{n}_i^x - [\![q^y]\!] n_i^y}{2\hat{a}}, \\
\mathbf{A}(\boldsymbol{u}_h; \xi_h^-, \xi_h^+) \cdot \boldsymbol{n}_i &\equiv \mathbf{q}^- \cdot \boldsymbol{n}_i + \lambda_1 \alpha_1 + \lambda_2 \alpha_2.
\end{aligned}$$

Note that, on any element, the outward normal $\boldsymbol{n}_e$ is either $\boldsymbol{n}_i$ or $-\boldsymbol{n}_i$, thus $\mathbf{A} \cdot \boldsymbol{n}_i$ is either $\mathbf{A} \cdot \boldsymbol{n}_e$ or $-\mathbf{A} \cdot \boldsymbol{n}_e$. Furthermore, if $k = 0$, the midpoint rule is used to approximate the integral

$$\langle \mathbf{A} \cdot \boldsymbol{n}_e, w \rangle_{\partial \Omega_e}.$$

That is, $\boldsymbol{u}_h, \xi_h^-$ and ξ_h^+ are evaluated at the midpoint of the edge in computing $\mathbf{A} \cdot \boldsymbol{n}_i$. If $k = 1$, two point Gaussian quadrature is used. The integration of the other terms

in (5) is exact, assuming that h_b is given as a continuou, piecewise linear interpolant of bathymetry data.

On elevation specified boundaries, the boundary condition is enforced through the flux $\mathbf{A} \cdot \boldsymbol{n}_e$ by setting ξ_h^+ equal to the specified elevation. On land boundaries, $\mathbf{A} \cdot \boldsymbol{n}_i$ is set to zero. On other boundaries, without any prior knowledge of ξ, we simply set $\xi_h^+ = \xi_h^-$.

Wetting and drying is implemented in (5) on each edge γ_i (unless this edge has already been designated a land edge). In particular, an edge is determined to be "wet" if $H^+ + H^- > 0$ and "dry" otherwise. For dry edges, we set $\mathbf{A} \cdot \boldsymbol{n}_i = 0$. For a wet edge, one of the elements on either side could be dry. If, for example, $H^+ \leq 0$, then we modify the computation of $\mathbf{A} \cdot \boldsymbol{n}_i$ by omitting the calculation of $\hat{\kappa}$, redefining $\hat{\boldsymbol{u}} = \boldsymbol{u}_h$, and proceeding with the calculations given above.

Implementation of (7). The implementation of the continuous Galerkin method (7) follows what has traditionally been done in ADCIRC [31]. In particular, mass lumping is employed in the first term, and explicit time stepping is used, except that $\pi\xi_h$ is evaluated at the new time level t^{n+1}.

3. Numerical results. In this section, we present numerical results for three domains: a quarter annular harbor, a section of the Mississippi River in southern Louisiana, and a constricted channel. The first test case is a standard test problem. The second test case involves significant wetting and drying, and the third test case tests the ability of the scheme to handle sharp gradients. We will compare the algorithm described above, implemented in a code which we refer to as the DG-ADCIRC code, to the standard GWCE implemention of ADCIRC, which we refer to as GWCE-ADCIRC. In all of the cases below, we have taken $k = 1$ in the DG scheme, though very similar results were obtained for $k = 0$. In each case, the units for elevation are in feet, and velocities are in feet/second.

3.1. Quarter Annular Harbor. The domain in this case is a quarter of an annulus. The finite element mesh of the domain is given in Figure 2, and consists of 2000 elements and 1066 nodes. The outer circular boundary is an open sea boundary, with elevation specified. The other three boundaries are land boundaries. The specified elevation is given by $\hat{\xi} = .1\cos(t\alpha)$ ft, where $\alpha = .000140518917083$, ramped up over a period of two days. The bathymetry for this test case is given in Figure 3.

The simulation was run for a total of 10 days, with a time step of 86.4 seconds. The elevation solution generated using the DG-ADCIRC code at ten days is given in Figure 4. Here we are plotting the projected solution $\pi\xi_h$. For comparison purposes, we have plotted the GWCE-ADCIRC solution in Figure 5. This solution is also a continuous, piecewise linear function. Very good agreement is seen between the two solutions. We have also compared the two components of velocity in Figures 6-7 and Figures 8-9. Here we see some differences in the solutions. Qualitatively the solutions are very similar; however, the GWCE-ADCIRC solutions are somewhat smoother than the DG-ADCIRC solutions. This may be dependent on our particular interpolation procedure (6), and the fact that velocities are dependent on $g\nabla\xi$. Thus, small differences in ξ can lead to larger relative differences in the velocity response.

We have also compared the DG-ADCIRC and GWCE-ADCIRC solutions at several "recording stations" located throughout the domain, over the time history of the simulation. Four stations in the computational domain were chosen, located at the points (235171, 24663.4) ft, (448615,151000) ft, (253065,232818) ft, and (49846.2,413298) ft. The first point is in the bottom part of the domain near the land boundary. The second point is near the open sea boundary. The third point is in the middle of the

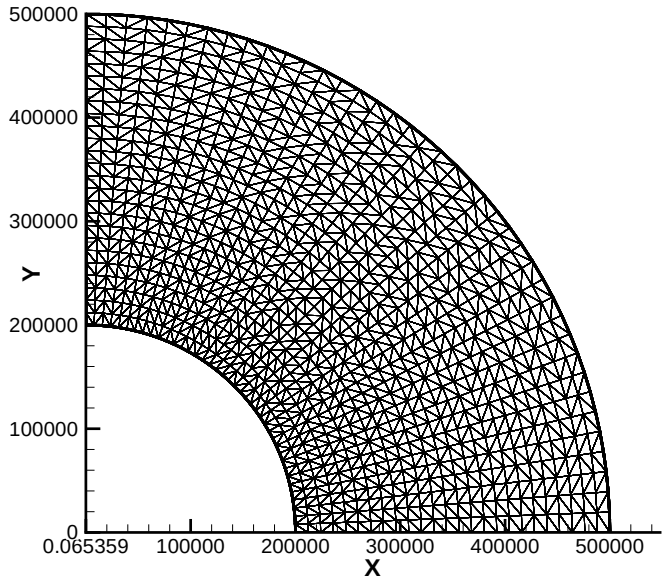

FIG. 2. *Finite element mesh for quarter annular harbor.*

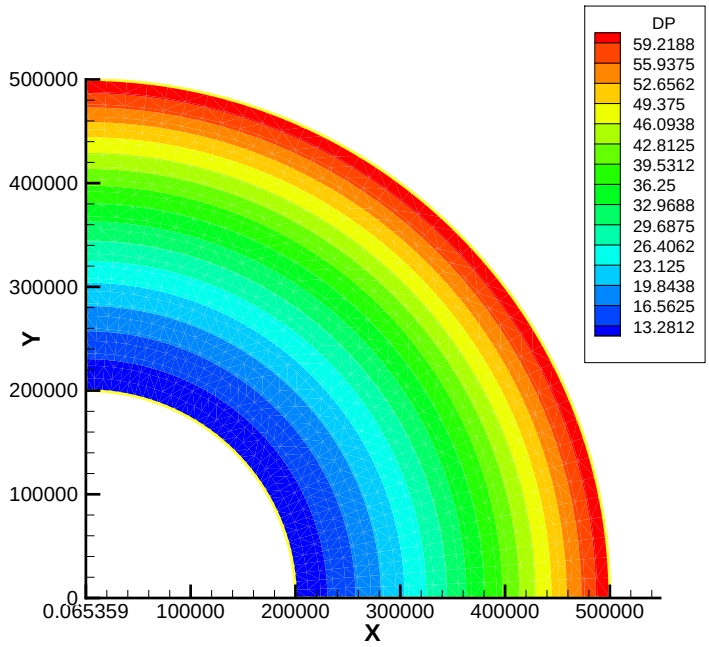

FIG. 3. *Bathymetry for quarter annular harbor.*

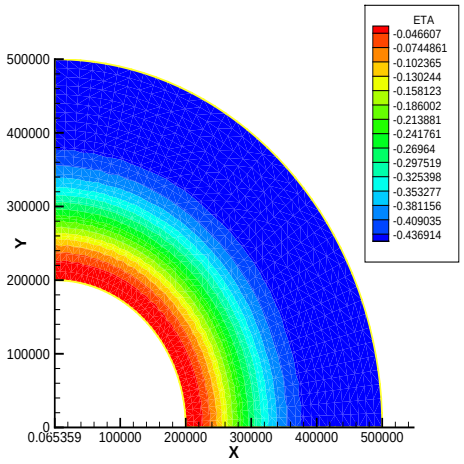

FIG. 4. *Elevation solution at ten days using DG-ADCIRC code for quarter annulus case.*

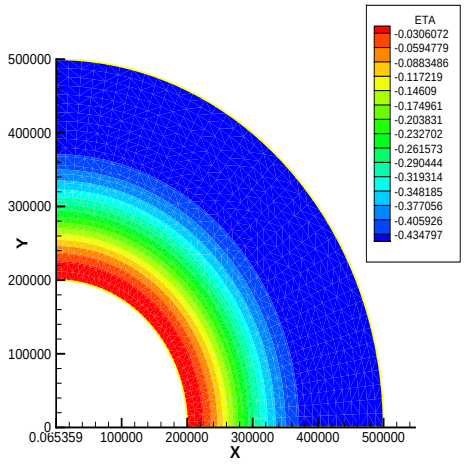

FIG. 5. *Elevation solution at ten days using GWCE-ADCIRC code for quarter annulus case.*

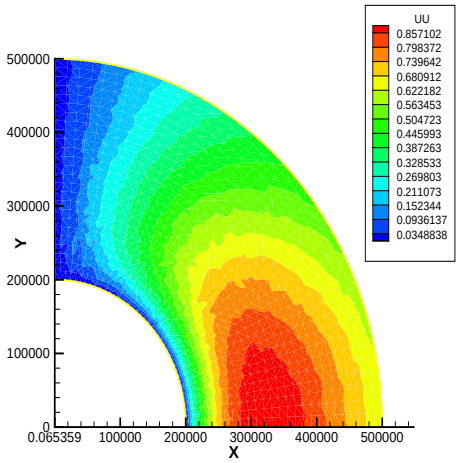

FIG. 6. *x velocity solution at ten days using DG-ADCIRC code for quarter annulus case.*

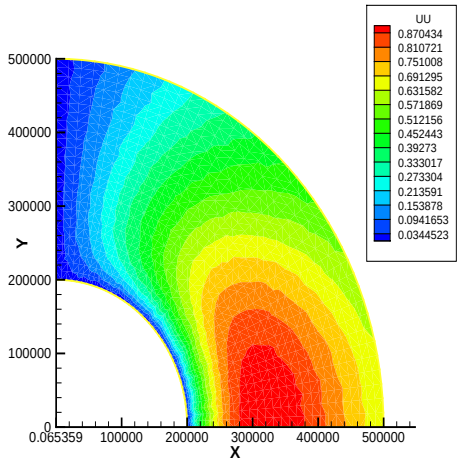

FIG. 7. *x velocity solution at ten days using GWCE-ADCIRC code for quarter annulus case.*

domain, and the fourth point is in the upper left part of the domain, also near the land boundary. The elevation solutions vs. time at all four locations is given in Figure 10. Excellent agreement is seen between the two solutions at all locations, in fact, they are indistinguishable. In Figures 11 and 12, we compare the x and y components of velocities at the four locations. Overall the two solutions agree quite well, except at the fourth node. Here we observe differences in the x component. At this location, however, the x component of velocity is relatively small compared to the magnitude of velocity at this point. The largest differences in velocity are about .014 ft/sec at this point, or about 2% relative to the magnitude of velocity at this point. Part of this difference could be due to the different ways land boundaries are incorporated in the GWCE and DG formulations.

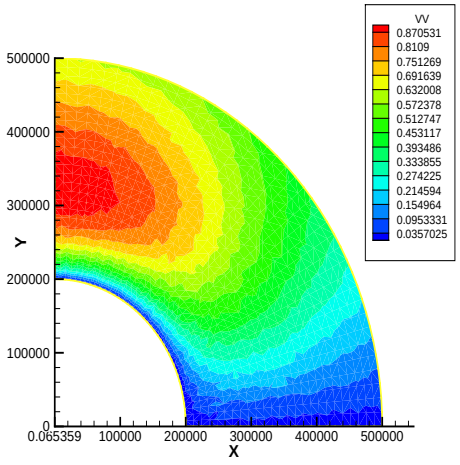

FIG. 8. *y velocity solution at ten days using DG-ADCIRC code for quarter annulus case.*

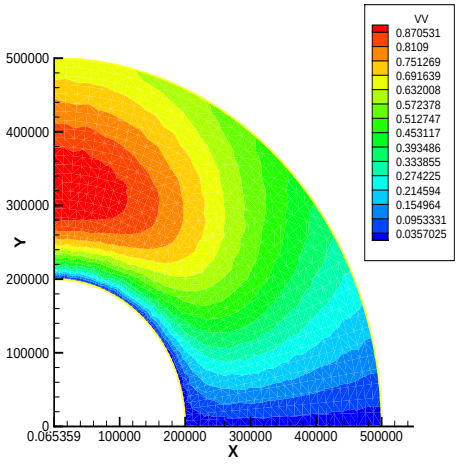

FIG. 9. *y velocity solution at ten days using GWCE-ADCIRC code for quarter annulus case.*

3.2. Mississippi River. The next test case involves a section of the Mississippi River near the Gulf Coast of Louisiana. The domain with initial water height is plotted in Figure 13. We zoom in on part of the domain in Figure 14. Portions of the domain are dry at the beginning of the simulation, as indicated by the negative bathymetries. As the simulation proceeds, a significant amount of wetting occurs throughout the domain. The finite element mesh consists of 35281 elements and 19616 nodes. For this test case, we simulated 2 days. A time step of .2 seconds was used in the GWCE-ADCIRC simulation. For stability purposes, a smaller time step of .1 seconds was used in the DG-ADCIRC simulation. An elevation boundary condition of 3.5 ft is specified at the northwest (upstream) entrance to the river section, and elevation of .61 ft is specified at the southeast (downstream) river boundary. This boundary condition is ramped up over a period of 1 day. All other boundaries are assumed to be land boundaries.

For this case, we compare elevation and velocity solutions at three recording stations, located at $(-3.473 * 10^7, 3.387 * 10^6)$ ft, $(-3.466 * 10^7, 3.342 * 10^6)$ ft and $(-3.463 * 10^7, 3.335 * 10^6)$ ft. These locations are at the upper left part of the domain (upstream) and about halfway and two-thirds downstream, respectively. First, we show the elevation solutions at the three locations, in Figure 15. Good agreement is seen between these solutions. Next, we compare the velocity solutions at the three locations, in Figure 16. Here we are comparing the solutions for the component of velocity with the larger magnitude at each location. Again, overall good agreement is seen between the two solutions. The DG-ADCIRC velocity solution exhibits some small fluctuations with time at the first station, which is near the inflow boundary.

3.3. Flow in a constricted channel. Our final test case involves flow in a constricted channel due to a step change in elevation. Initially we assume the water is stationary. Then at $t > 0$, we raise the elevation at the left boundary to .1 feet. This induces flow from left to right, down the constricted channel. The purpose of this example is to test the DG-ADCIRC code's ability to handle a sudden change in elevation. The domain with the finite element mesh is shown in Figure 17. The mesh contains 3155 elements and 1670 nodes. Land boundaries are assumed on the top,

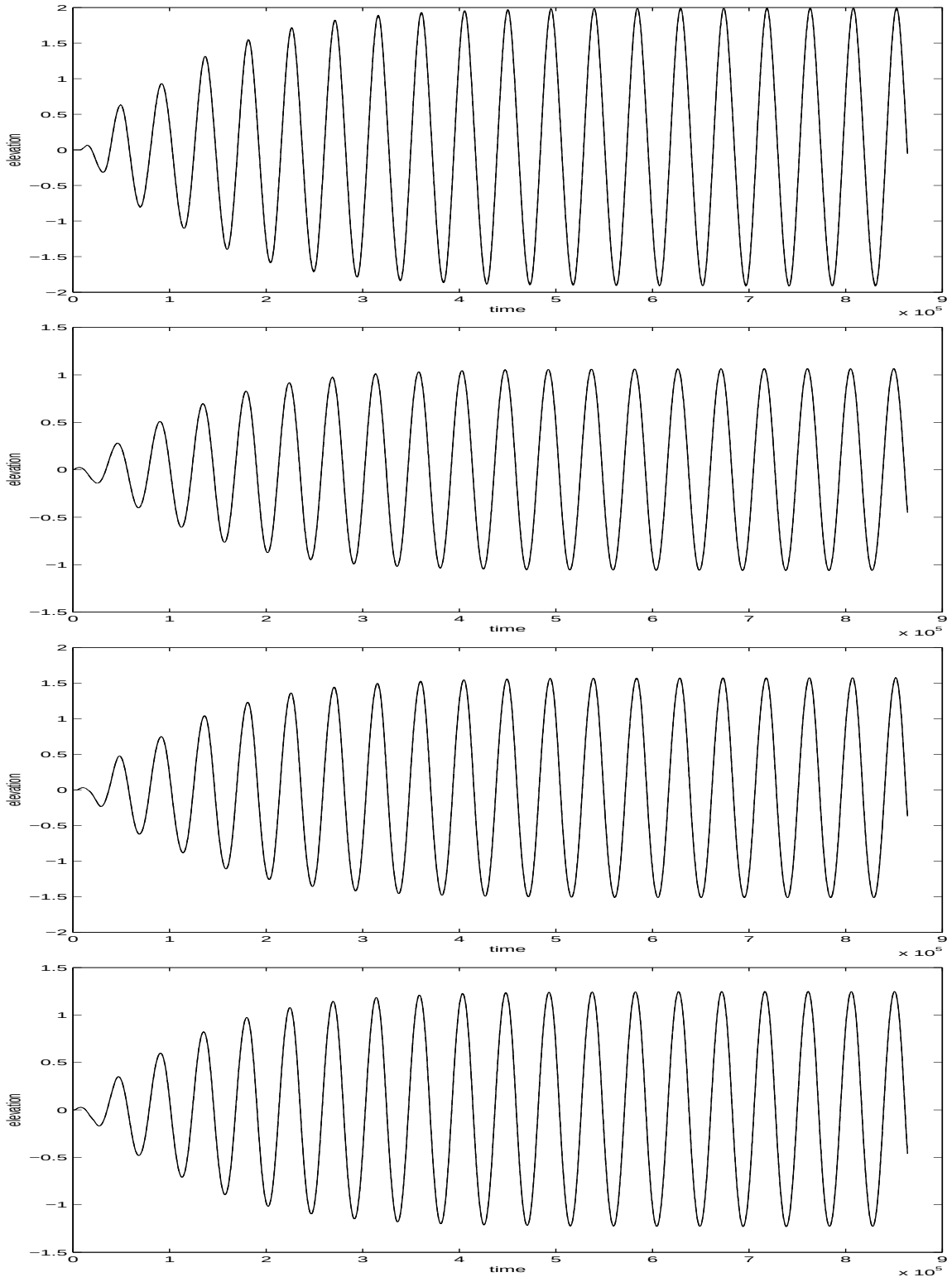

FIG. 10. *Comparison of elevation solutions at days 0-10 for quarter annulus case. GWCE-ADCIRC solution is solid line, DG-ADCIRC solution is dashed line.*

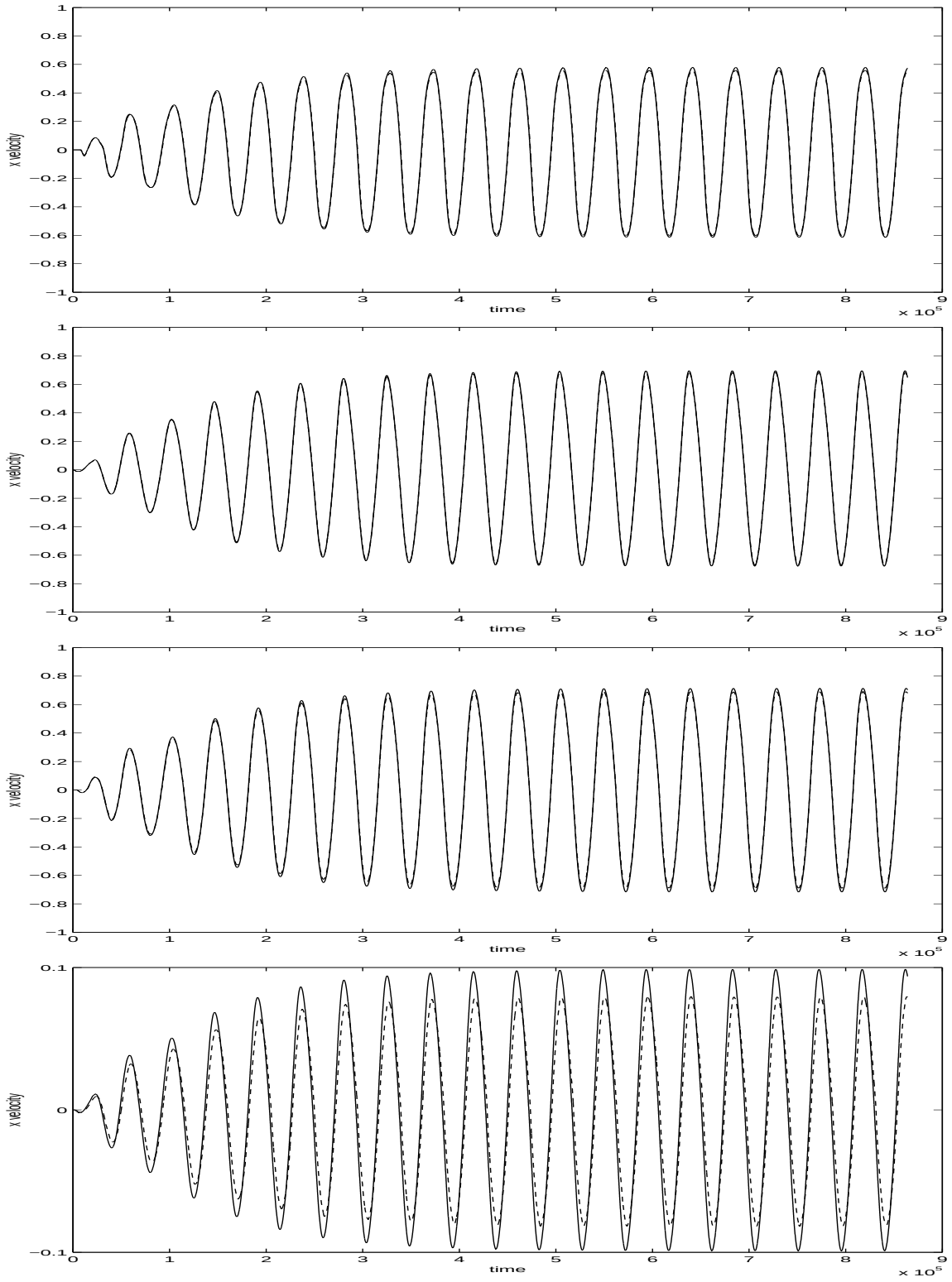

FIG. 11. *Comparison of x velocity solutions at days 0-10 for quarter annulus case. GWCE-ADCIRC solution is solid line, DG-ADCIRC solution is dashed line.*

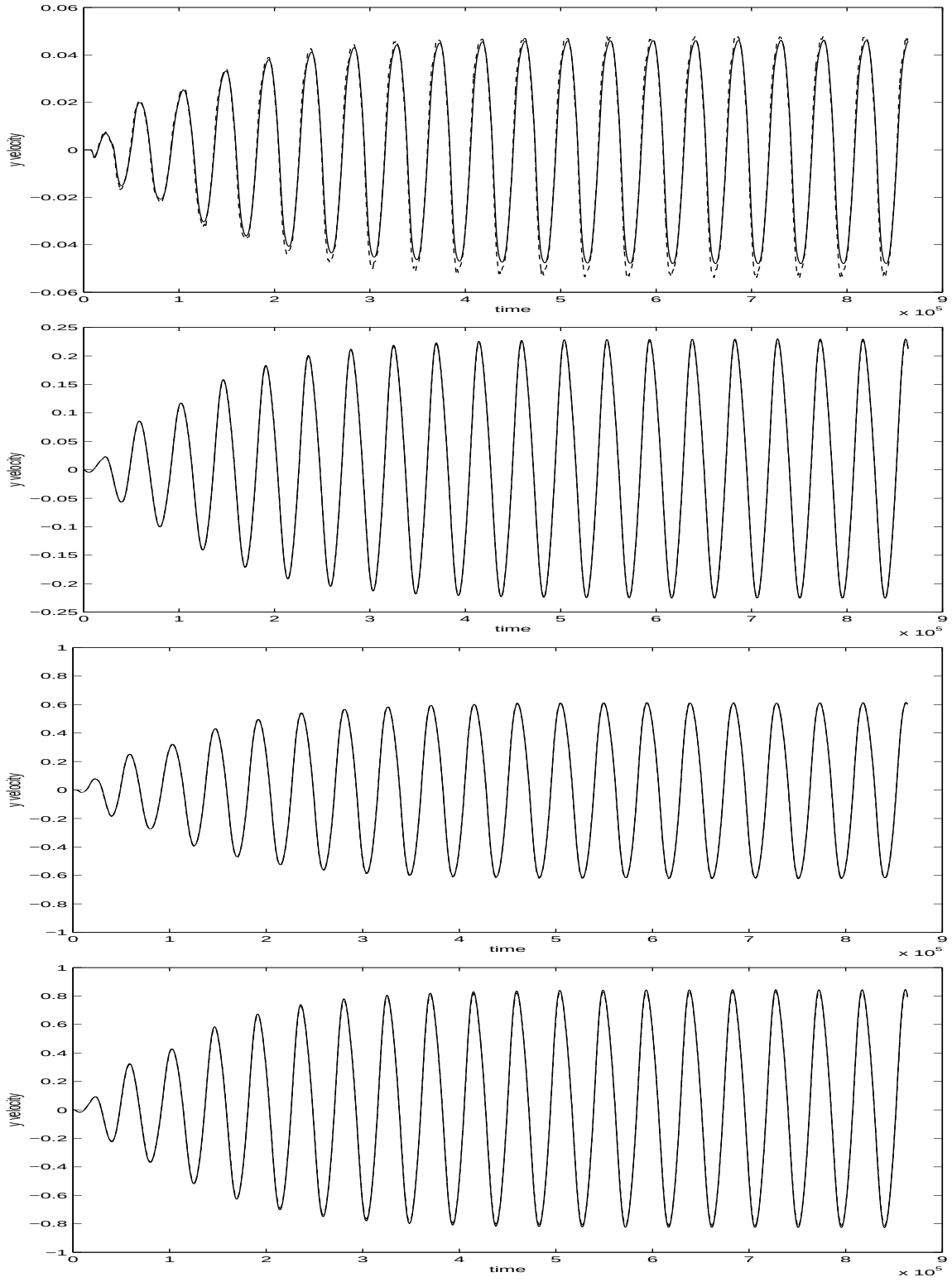

FIG. 12. *Comparison of y velocity solutions at days 0-10 for quarter annulus case. GWCE-ADCIRC solution is solid line, DG-ADCIRC solution is dashed line.*

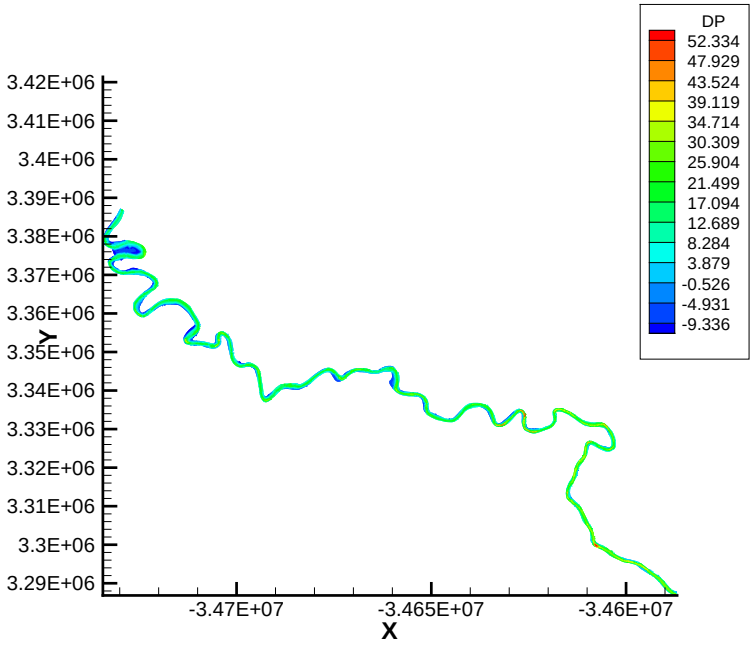

FIG. 13. *Mississippi River bathymetry.*

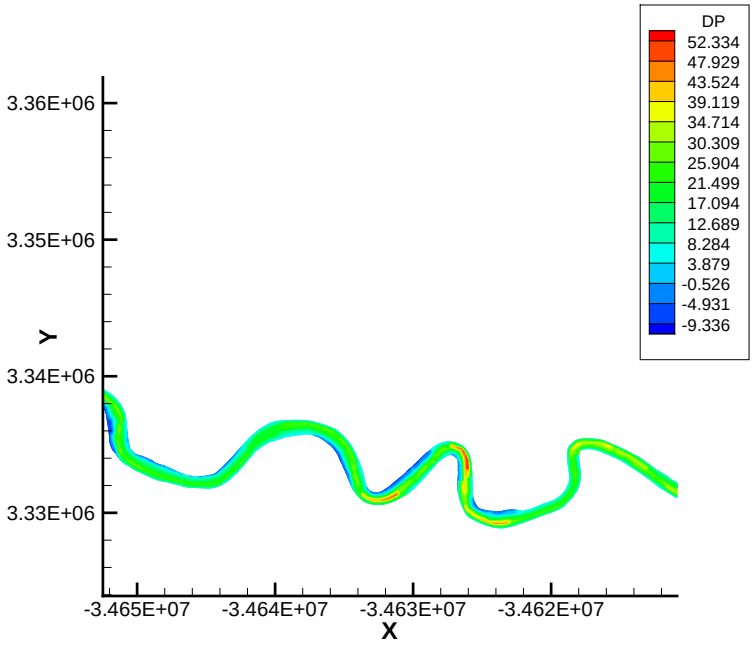

FIG. 14. *Zoom in on Mississippi River bathymetry.*

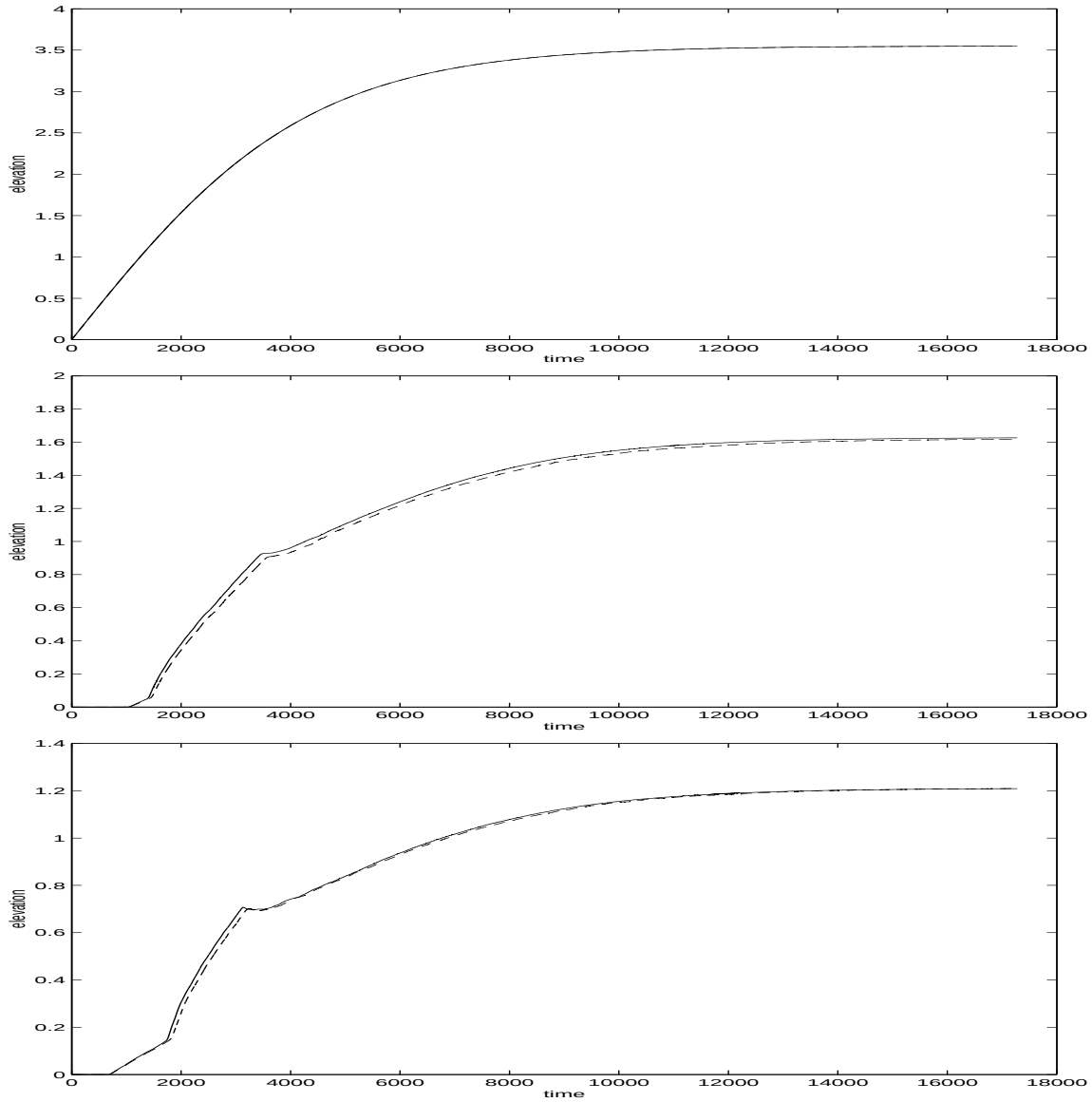

FIG. 15. *Comparison of elevation solutions at days 0-2 for Mississippi River case. GWCE-ADCIRC solution is solid line, DG-ADCIRC solution is dashed line.*

bottom and right boundaries. A constant bathymetry of 1 ft is assumed. A time step of .02 seconds was used.

In Figure 18, we compare the GWCE-ADCIRC and DG-ADCIRC elevation solutions at $t = 400$ seconds. The GWCE solution in this case is quite oscillatory, exhibiting a significant amount of rippling downstream of the front. The DG solution exhibits a more stable, sharp profile. Solutions at $t = 600$ and $t = 800$ seconds are shown in Figures 19 and 20. Similar results are seen in these figures. Finally, in Figure 21, we compare the elevation and x velocity solutions at the point (-1.26,20.34) ft vs. time for the two methods. The DG solution is clearly superior for this case.

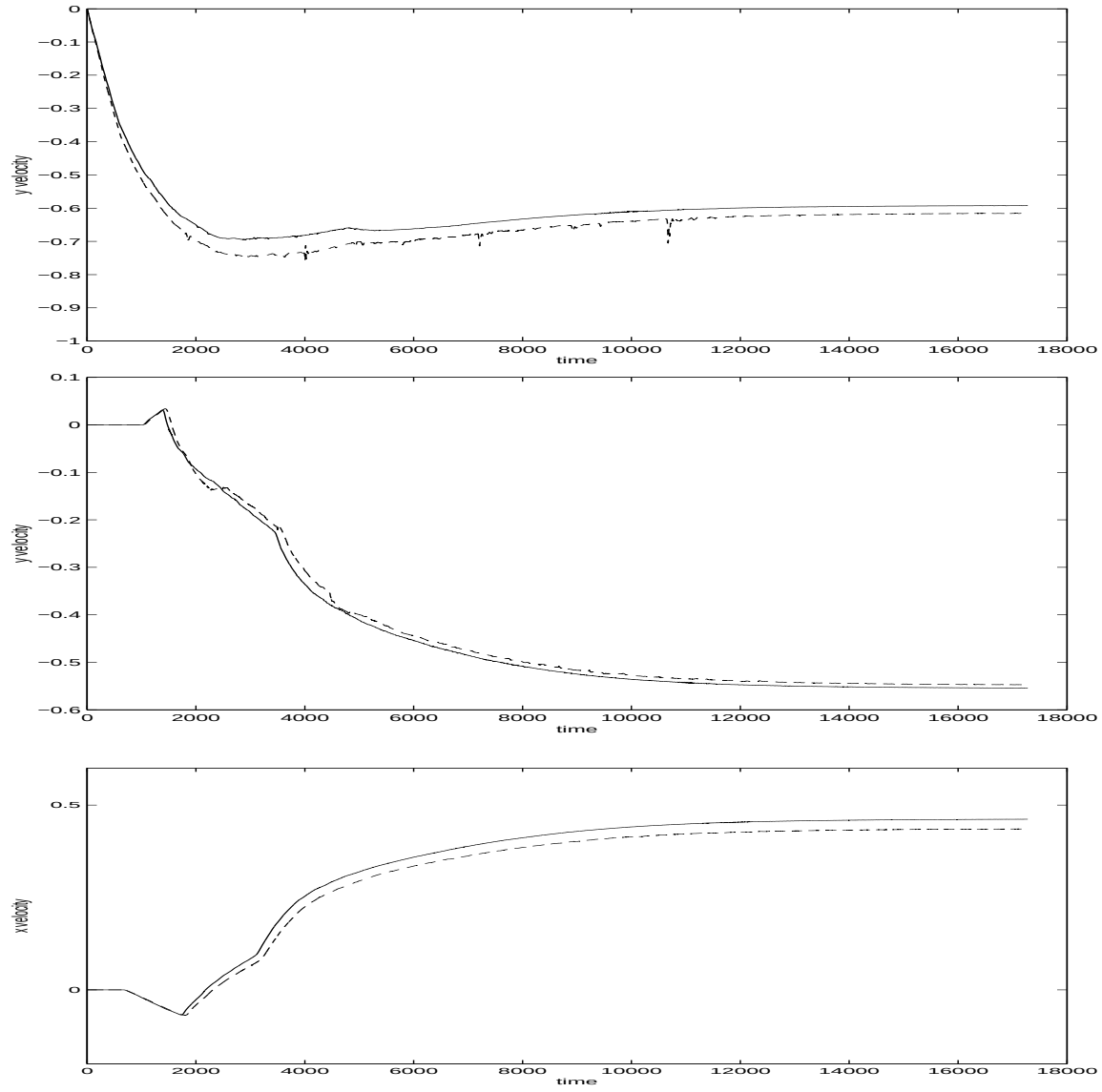

FIG. 16. *Comparison of velocity solutions at days 0-2. GWCE-ADCIRC solution is solid line, DG-ADCIRC solution is dashed line for Mississippi River case.*

3.4. Summary of results. In summary, for the cases tested so far with fairly smooth solutions, we have observed very similar results between the DG-ADCIRC and GWCE-ADCIRC codes. In some cases, the velocity solutions differ, but these differences are relatively small. As the solution gradients become steeper, the DG-ADCIRC code does not seem to exhibit the same oscillations as the GWCE-ADCIRC code does. As the DG method has built-in upwinding and shock-capturing capabilities, this is not surprising. Moreover, the DG solution has the added feature of being locally conservative and flux-continuous.

In terms of computational cost, the DG method on the same finite element mesh

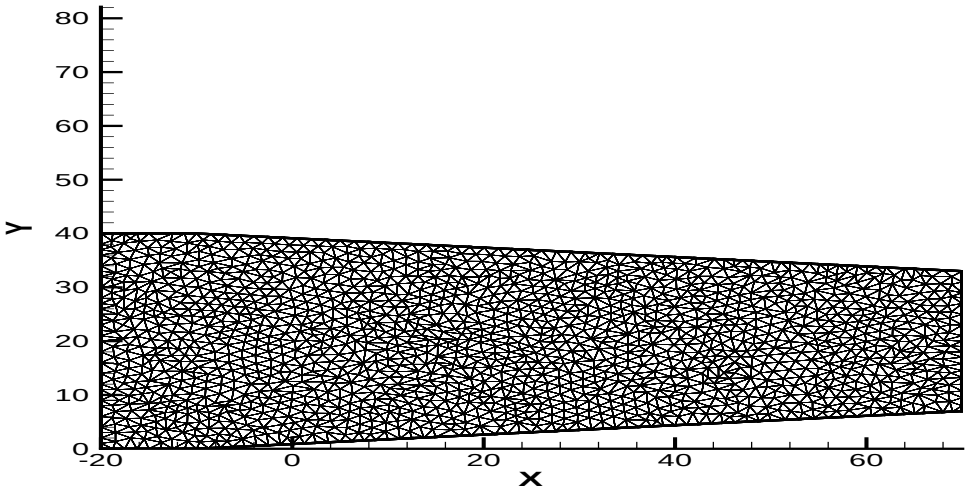

FIG. 17. *Constricted channel with finite element mesh.*

involves more degrees of freedom per solution step than the GWCE formulation. However, the GWCE involves solving a system of equations at every step. While these systems can be solved very efficiently using a preconditioned conjugate gradient method, generally 3-10 conjugate gradient iterations are required per time step, depending on the problem size. In some cases, the DG method requires a smaller time step than the GWCE method in order for the solution to remain stable, generally about half the size. But, for the cases considered so far, the wall-clock timings between the two methods are quite comparable.

4. Conclusions. In this paper, we have presented a numerical approach for the SWE based on combining a DG finite element method for the primitive continuity equation and a continuous Galerkin finite element method for the momentum equation. The DG formulation is locally conservative and flux continuous. Preliminary numerical results indicate the new methodology is competitive with existing methodologies for smooth flow and wetting and drying problems, and produces superior results in cases with steep elevation gradients.

5. Acknowledgments. The authors would like to acknowledge Jennifer Proft for her help in generating the numerical results.

REFERENCES

[1] V. AIZINGER AND C. DAWSON, *Discontinuous Galerkin methods for two-dimensional flow and transport in shallow water*, Advances in Water Reources, 25 (2002), pp. 67–84.

[2] F. ALCRUDO AND P. GARCIA-NAVARRO, *A high-resolution godunov-type scheme in finite volumes for the 2d shallow-water equations*, Int. J. Num. Meth. Fluids, 16 (1993), pp. 489–505.

[3] C. BAUMANN AND J. ODEN, *A discontinuous hp finite element method for convection-diffusion problems*, in Comput. Methods Appl. Mech. Engrg., special issue on Spectral, Spectral Element, and *hp* Methods in CFD, M. A. G.E. Karniadakis and C. Bernardi, eds., in press.

[4] K. S. BEY AND J. T. ODEN, *hp-version discontinuous Galerkin methods for hyperbolic conservation laws*, Comput. Methods Appl. Mech. Engrg., 133 (1996), pp. 259–286.

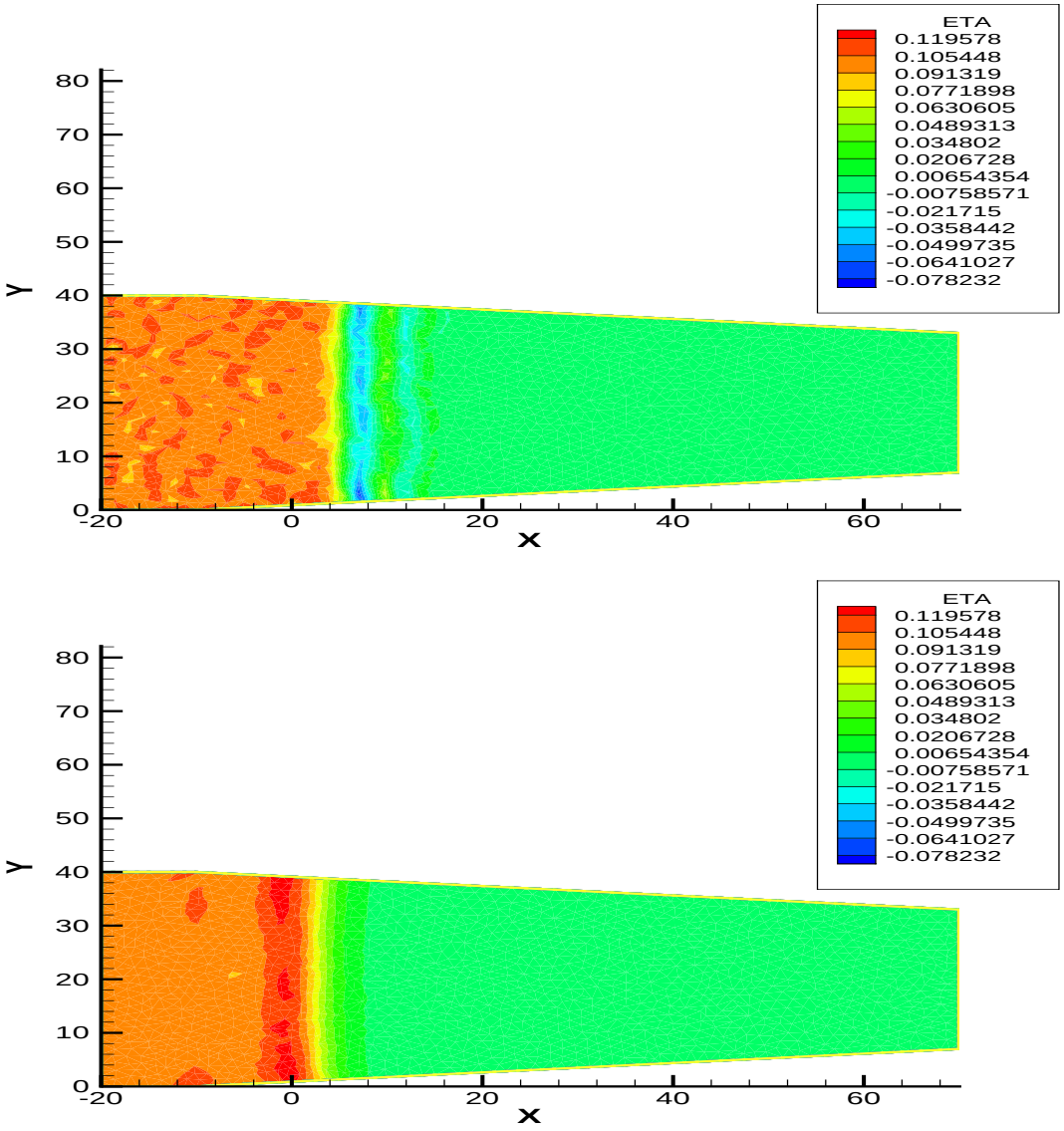

FIG. 18. *Comparison of elevation solutions at $t = 400$ seconds for constricted channel case. GWCE-ADCIRC solution is top graph, DG-ADCIRC solution is the bottom one.*

[5] C. A. BLAIN, J. J. WESTERINK, AND R. A. LUETTICH, *The influence of domain size on the response characteristics of a hurricane storm surge model*, Journal of Geophysical Research, 99, C9 (1994), pp. 18467–18479.

[6] ———, *Grid convergence studies for the prediction of hurricane storm surges*, Int. J. Num. Meth. Fluids, 26 (1998), pp. 369–401.

[7] P. CASTILLO, B. COCKBURN, I. PERUGIA, AND D. SCHÖTZAU, *An a priori error analysis of the local discontinuous Galerkin method for elliptic problems*, SIAM J. Numer. Anal., (to appear).

[8] S. CHIPPADA, C. N. DAWSON, M. L. MARTÍNEZ, AND M. F. WHEELER, *Finite element approximations to the system of shallow water equations, Part I: Continuous time a priori error estimates*, SIAM J. Numer. Anal., 35 (1998), pp. 692–711.

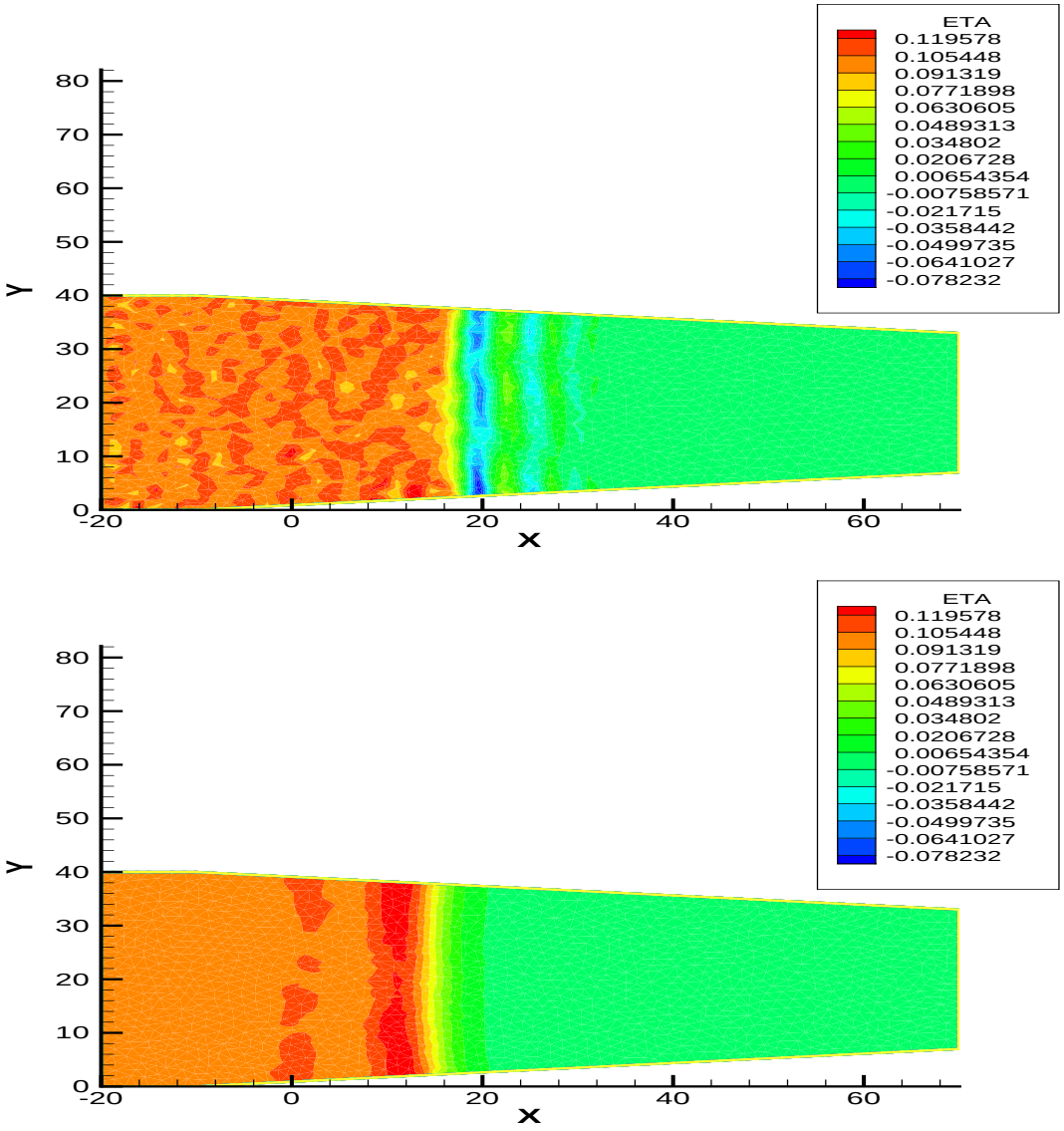

FIG. 19. *Comparison of elevation solutions at $t = 600$ seconds for constricted channel case. GWCE-ADCIRC solution is top graph, DG-ADCIRC solution is the bottom one.*

[9] ———, *Finite element approximations to the system of shallow water equations, Part II: Discrete time a priori error estimates*, SIAM J. Numer. Anal., 35 (1998), pp. 1790–1724.

[10] ———, *A godunov-type finite volume method for the system of shallow water equations*, Comput. Meth. Appl. Mech. Engrg., 151 (1998), pp. 105–129.

[11] B. COCKBURN AND C. DAWSON, *Some extensions of the local discontinuous Galerkin method for convection-diffusion equations in multidimensions*, in The Proceedings of the Conference on the Mathematics of Finite Elements and Applications: MAFELAP X, J. Whiteman, ed., Elsevier, 2000.

[12] B. COCKBURN, S. HOU, AND C. SHU, *TVB Runge-Kutta local projection discontinuous Galerkin finite element method for conservation laws IV: The multidimensional case*, Math. Comp., 54 (1990), pp. 545–581.

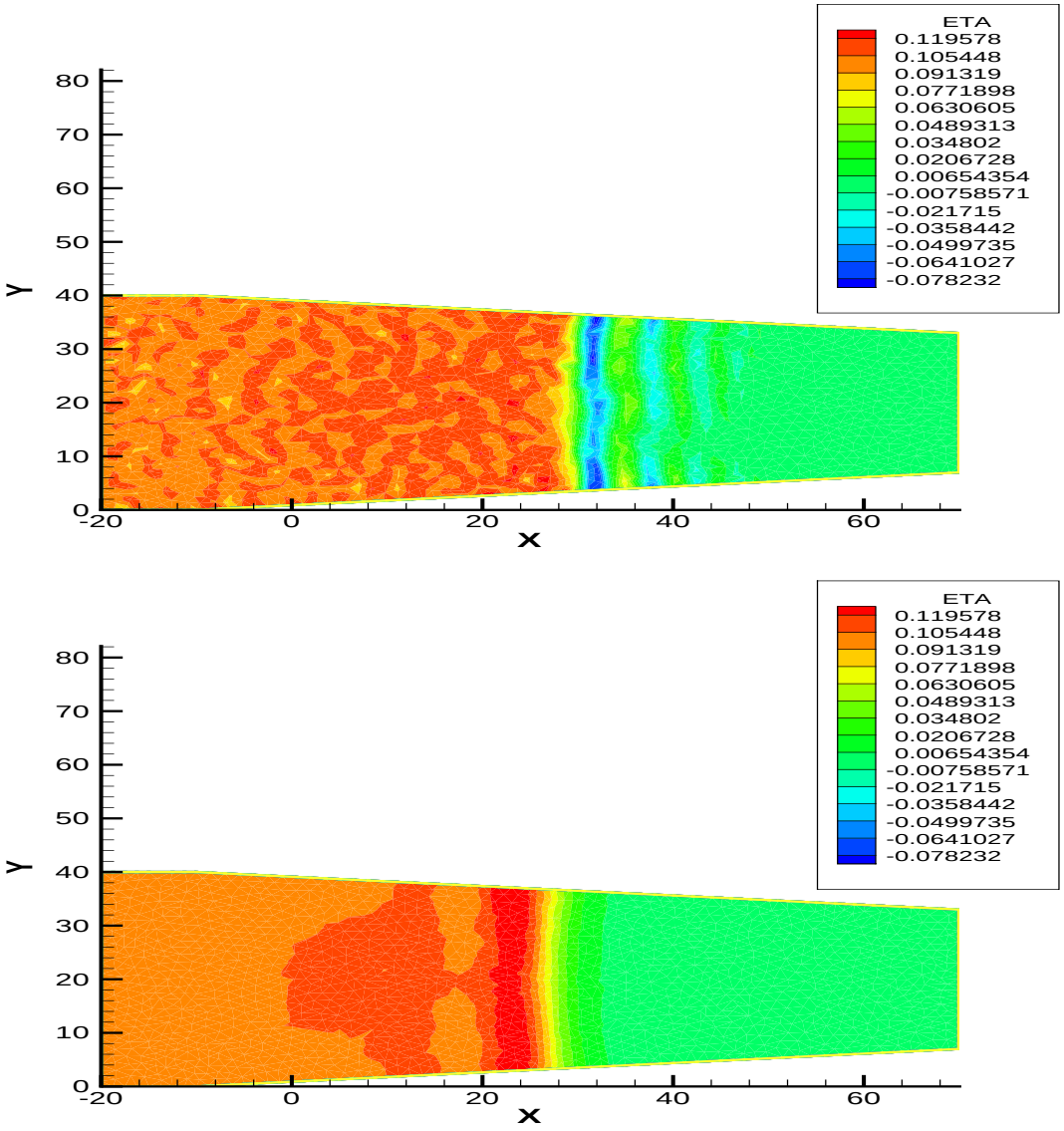

FIG. 20. *Comparison of elevation solutions at $t = 800$ seconds for constricted channel case. GWCE-ADCIRC solution is top graph, DG-ADCIRC solution is the bottom one.*

[13] B. COCKBURN, G. KARNIADAKIS, AND C.-W. SHU, *The development of discontinuous Galerkin methods*, in First International Symposium on Discontinuous Galerkin Methods, Lecture Notes in Computational Science and Engineering, B. Cockburn, G. Karniadakis, and C.-W. Shu, eds., vol. 11, Springer Verlag, February 2000, pp. 3–50.

[14] B. COCKBURN, S. LIN, AND C. SHU, *TVB Runge-Kutta local projection discontinuous Galerkin finite element method for conservation laws III: One dimensional systems*, J. Comput. Phys., 84 (1989), pp. 90–113.

[15] B. COCKBURN AND C. SHU, *TVB Runge-Kutta local projection discontinuous Galerkin finite element method for scalar conservation laws II: General framework*, Math. Comp., 52 (1989), pp. 411–435.

[16] ———, *The Runge-Kutta local projection P^1-discontinuous Galerkin method for scalar conser-*

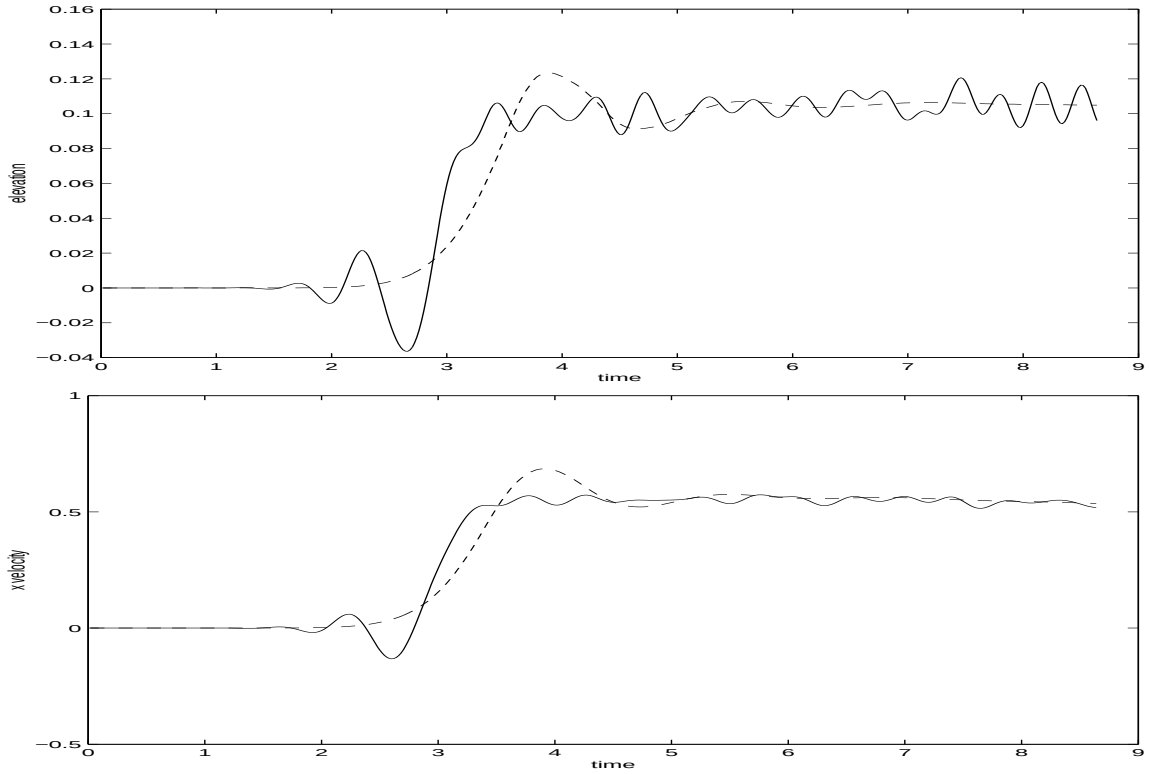

FIG. 21. *Comparison of elevation and velocity solutions vs. time at the point (-1.26,20.34) ft, for constricted channel case. GWCE-ADCIRC solution is the solid line, DG-ADCIRC solution is the dashed line.*

vation laws, RAIRO Modél. Math. Anal.Numér., 25 (1991), pp. 337–361.

[17] ———, *The local discontinuous Galerkin finite element method for convection-diffusion systems*, SIAM J. Numer. Anal., 35 (1998), pp. 2440–2463.

[18] ———, *The Runge-Kutta discontinuous Galerkin finite element method for conservation laws V: Multidimensional systems*, J. Comput. Phys., 141 (1998), pp. 199–224.

[19] C. DAWSON, *Conservative, shock-capturing transport methods with nonconservative velocity approximations*, Computational Geosciences, 3 (1999), pp. 205–227.

[20] C. DAWSON AND J. PROFT, *A priori error estimates for interior penalty versions of the local discontinuous Galerkin method applied to transport equations*, Numerical Methods for Partial Differential Equations, 17 (2001), pp. no. 6, 545–564.

[21] ———, *Discontinuous and coupled continuous/discontinuous Galerkin methods for the shallow water equations*, Comp. Meth. Appl. Mech. Eng., (to appear).

[22] M. G. G. FOREMAN, *An analysis of the wave equation model for finite element tidal computations*, Computational Physics, 52 (1983), pp. 290–312.

[23] ———, *A comparison of tidal models for the southwest coast of Vancouver Island*, in Computational Methods in Water Resources: Proceedings of the VII International Conference, MIT, M. A. Celia, ed., Elsevier, 1988.

[24] W. G. GRAY, *A finite element study of tidal flow data for the North Sea and English Channel*, Advances in Water Resources, 12 (1989), pp. 143–154.

[25] W. G. GRAY, J. DROLET, AND I. P. E. KINNMARK, *A simulation of tidal flow in the southern part of the North Sea and the English Channel*, Advances in Water Resources, 10 (1987), pp. 131–137.

[26] M. KAWAHARA, H. HIRANO, K. TSUHORA, AND K. IWAGAKI, *Selective lumping finite element method for shallow water equations*, Int. J. Num. Meth. Eng., 2 (1982), pp. 99–112.

[27] I. KING AND W. R. NORTON, *Recent application of RMA's finite element models for two-dimensional hydrodynamics and water quality*, in Finite Elements in Water Resources II,

C. Brebbia, W.G.Gray, and G.F.Pinder, eds., Pentech Press, London, 1978.

[28] I. P. E. Kinnmark, *The Shallow Water Wave Equations: Formulation, Analysis, and Application*, Ph. D. thesis, Department of Civil Engineering, Princeton University, (1984).

[29] R. Kolar, J. Westerink, M. Cantekin, and C. Blain, *Aspects of nonlinear simulations using shallow water models based on the wave continuity equation*, Computers and Fluids, 23, 3 (1994), pp. 523–538.

[30] R. J. LeVeque, *Numerical Methods for Conservation Laws*, Lectures in Mathematics, Birkhauser Verlag, Basel, 1992.

[31] R. A. Luettich, J. J. Westerink, and N. W. Scheffner, *ADCIRC: An advanced three-dimensional circulation model for shelves, coasts and estuaries, Report 1: Theory and methodology of ADCIRC-2DDI and ADCIRC-3DL*, in Dreding Research Program Technical Report DRP-92-6, U.S. Army Engineers Waterways Experiment Station, Vicksburg, MS, 1992.

[32] D. R. Lynch and W. R. Gray, *A wave equation model for finite element computations*, Computers and Fluids, 7 (1979), pp. 207–228.

[33] J. Oden, I. Babuška, and C. Baumann, *A discontinuous hp finite element method for diffusion problems*, J. Comput. Phys., 146 (1998), pp. 491–519.

[34] B. Rivière, M. Wheeler, and V. Girault, *Improved energy estimates for interior penalty, constrained and discontinuous Galerkin methods for elliptic problems. Part I*, Computational Geosciences, 3 (1999), pp. 337–360.

[35] R. Szymkiewicz, *Oscillation-free solution of shallow water equations for nonstaggered grid*, J. Hyd. Engg., 119 (1993), pp. 1118–1137.

[36] T. Weiyan, *Shallow Water Hydrodynamics*, vol. 55 of Elsevier Oceanography Series, Elsevier, Amsterdam, 1992.

[37] F. Werner and D. R. Lynch, *Field verification of wave equation tidal dynamics in the English Channel and southern North Sea*, Advances in Water Resources, 10 (1987), pp. 115–130.

[38] ———, *Harmonic structure of English Channel/Souther Bight tides from a wave equation simulation*, Advances in Water Resources, 12 (1989), pp. 121–142.

[39] J. J. Westerink, R. A. Luettich, A. M. Baptista, N. W. Scheffner, and P. Farrar, *Tide and storm surge predictions using a finite element model*, J. Hydraulic Eng., 118 (1992), pp. 1373–1390.

[40] J. J. Westerink, R. A. Luettich, and R. L. Kolar, *Advances in finite element modeling of coastal ocean hydrodynamics*, in 11th International Conference on Computational Methods in Water Resources, Computational Mechanics Publications, Southampton, U.K., 1996.

[41] M. Wheeler, *An elliptic collocation-finite element method with interior penalties*, SIAM J. Numer. Anal., 15 (1978), pp. 152–161.

[42] O. Zienkiewicz and P. Ortiz, *A split-characteristic based finite element model for the shallow water equations*, Int. J. Num. Meth. Fluids, 20 (1995), pp. 1061–1080.